Pre-Intercalation of Squaric Acid to Construct V-O-C Bonding: Boosting Zn^{2+} Storage in $H_{11}Al_2V_6O_{23.2}$ Cathode

Zihan Wang[a], Qiande Liu[a], Xin Yu[a], Siyu Song[a], Yusheng Wu[a], Fang Hu[a]*, Kai Zhu[b]*

[a] College of Materials Science and Engineering, Shenyang University of Technology, Shenyang Key Laboratory of Advanced Energy Materials and Renewable Resources, Shenyang 110870, Liaoning, China

[b] Key Laboratory of Superlight Materials and Surface Technology of Ministry of Education, College of Materials Science and Chemical Engineering, Harbin Engineering University, Harbin 150010, Heilongjiang, China

*Corresponding authors. E-mail addresses: hufang25@sut.edu.com (F. Hu), kzhu@hrbeu.edu.cn (K. Zhu).

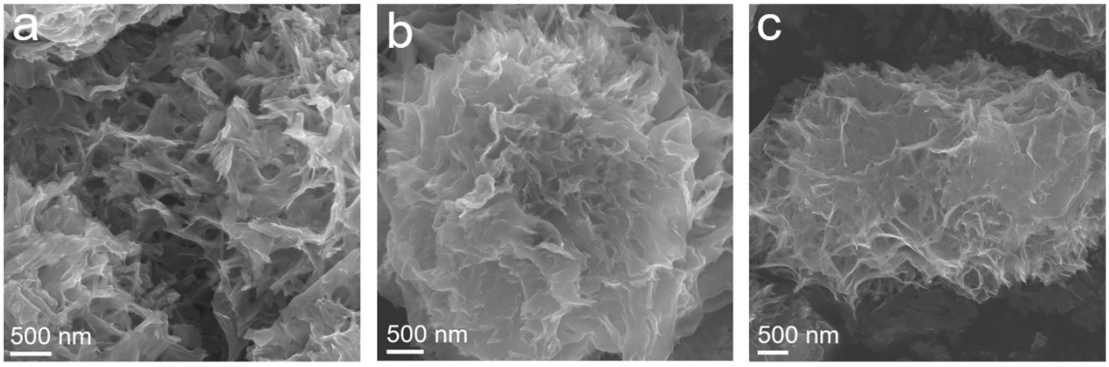

Fig. S1. SEM images of HAVO (a), HAVO-Sq40 (b), HAVO-Sq120 (c).

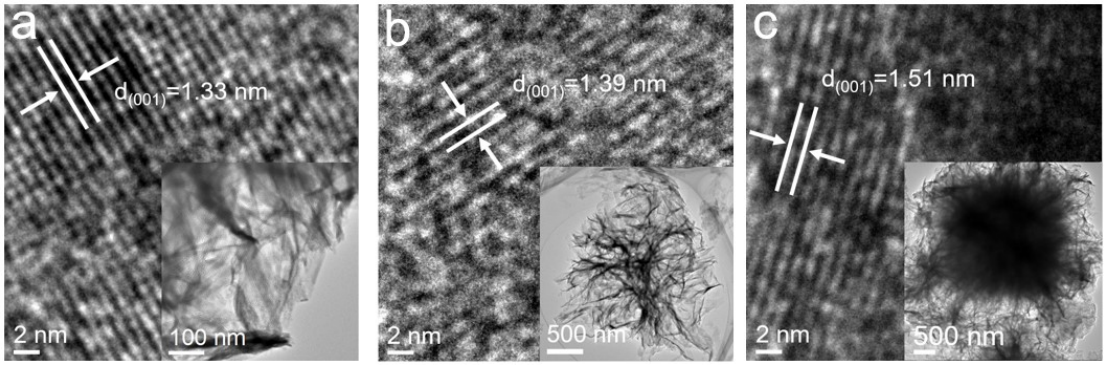

Fig. S2. HR-TEM images of HAVO (a), HAVO-Sq40 (b), HAVO-Sq120 (c).

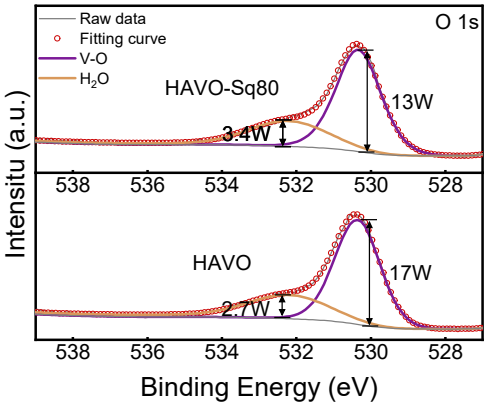

Fig. S3. O 1s XPS spectra of HAVO and HAVO-Sq80.

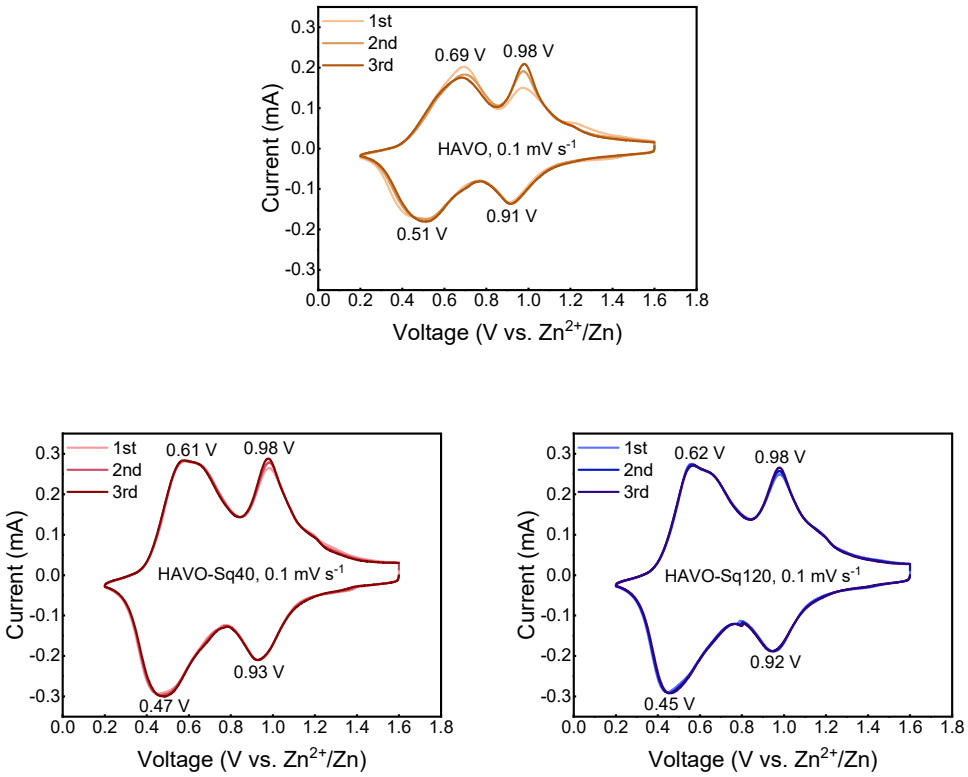

Fig. S4. CV curves of HAVO, HAVO-Sq40 and HAVO-Sq120.

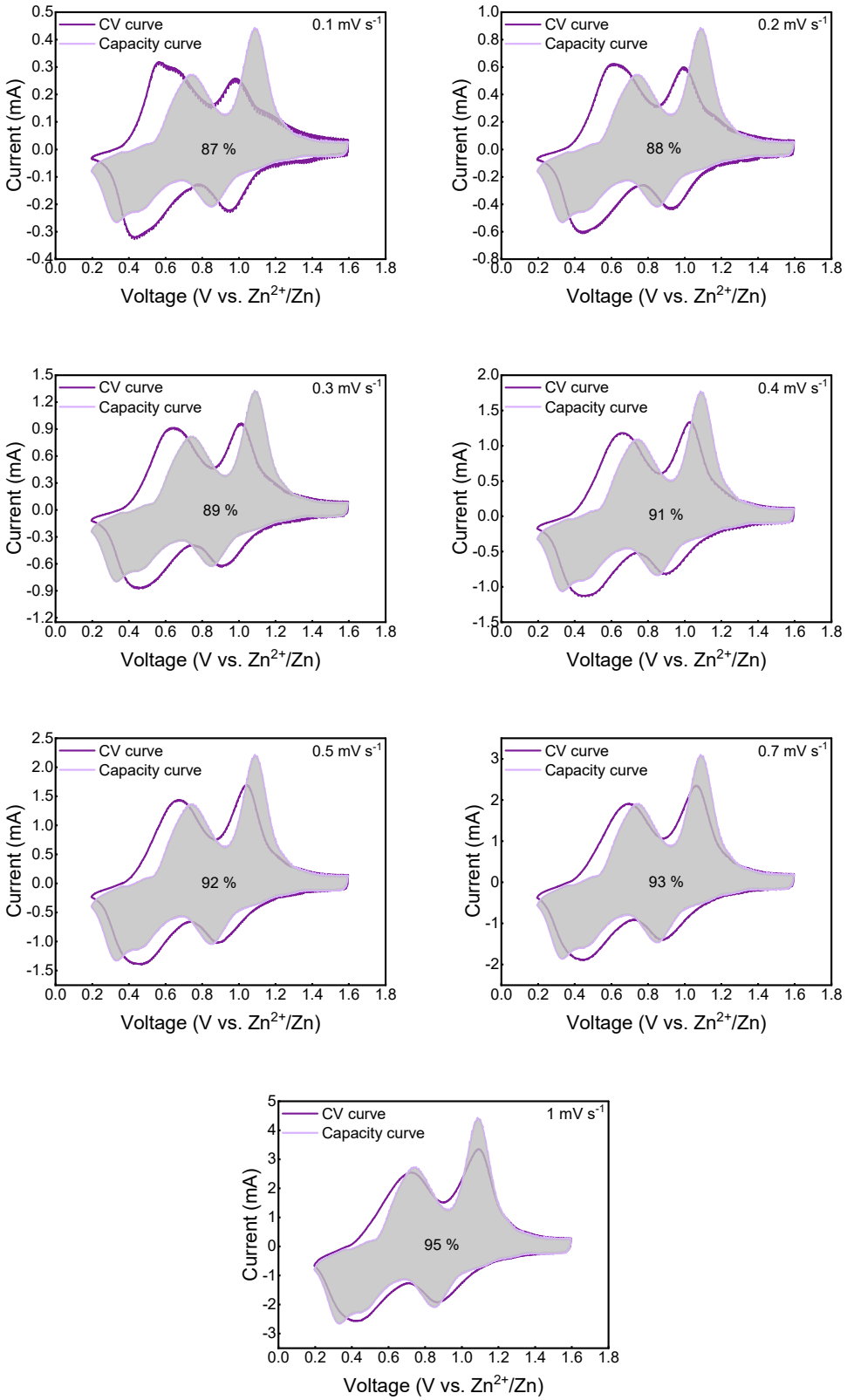

Fig. S5. Capacitive (gray area) contributions for HAVO-Sq80 at different scan rates.

The specific change in peak position is in the form of a shift of the cathodic and anodic peaks to higher and lower voltages respectively. The relationship between test current and sweep rate is shown in equation (1) below:

$$i = av^b \ (\log(i) = \log(a) + b\log(v)) \quad (1)$$

In equation (1), a and b are variables, i is the test current when the scan rate is v. Typically the value of b-value is in the range 0.5-1.0, and Values of b close to 1 and 0.5 indicate that the electrochemical process is controlled by surface pseudo-capacitance and diffusion, respectively.

The Zn^{2+} storage mechanism can be divided into diffusion-controlled and capacitance-controlled processes, depending on the scanning rate. As shown in equation (2):

$$i = k_1 v + k_2 v^{1/2} \quad (2)$$

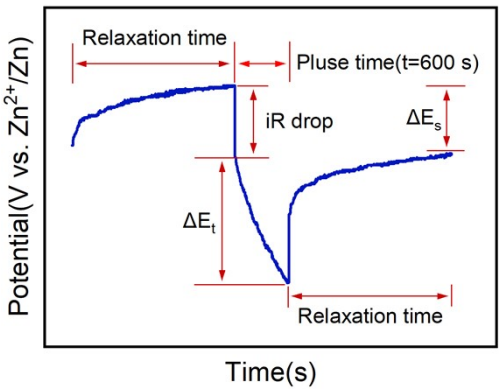

Fig, S6 E Vs. t profile of the electrode for a single GITT during discharge process.

Which as composed of 10 min galvanostatic charge (pluse) at 0.1 A g^{-1}, and followed by 60 min relaxation time. The iR drop as shown along with the ΔE_t and ΔE_s

To further reveal the reason for the high-performance of the full cells, the galvanostatic intermittent titration technique (GITT) measurement was carried out to determine the Zn^{2+} diffusion coefficient, as shown in Fig. S5. The cell was discharged or charged at the current density of 0.1 A g^{-1} for an interval of 10 min and then relaxed for 60 min to allow the voltage to reach equilibrium. The procedure was repeatedly applied to the cell during the entire charge/discharge process. The Zn^{2+} diffusion coefficient can be calculated based on the following equation:

$$D = \frac{4L^2}{\pi\tau}\left(\frac{\Delta E_s}{\Delta E_t}\right)^2$$

Where t is the duration of the current pulse (s), τ is the relaxation time (s), and ΔE_s is he steady-state potential change (V) by the current pulse. ΔE_t is the potential change (V) during the constant current pulse after eliminating the iR drop. L is zinc ion diffusion length (cm); for compact electrode, it is equal to the thickness of the electrode.

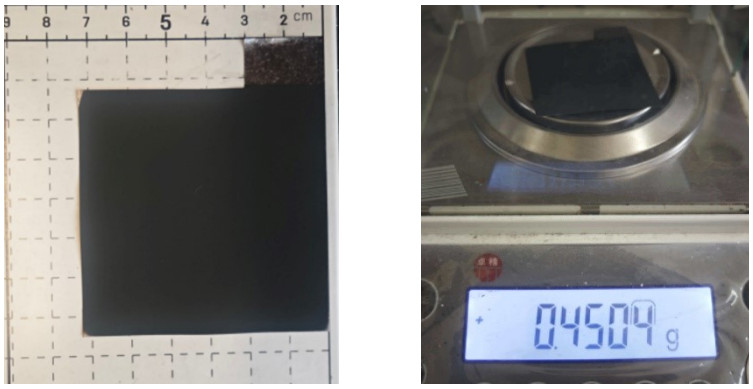

Fig. S7. Optical photo of electrode.

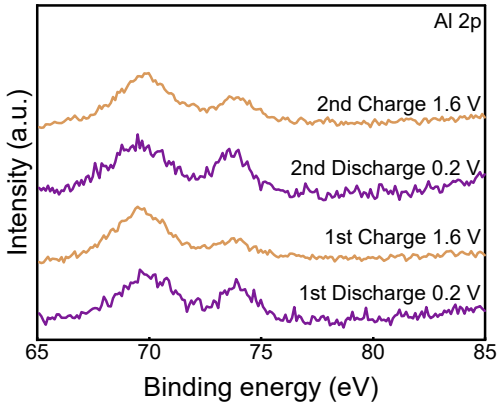

Fig. S8. Ex-situ Al 2p XPS specrta of HAVO-Sq80.

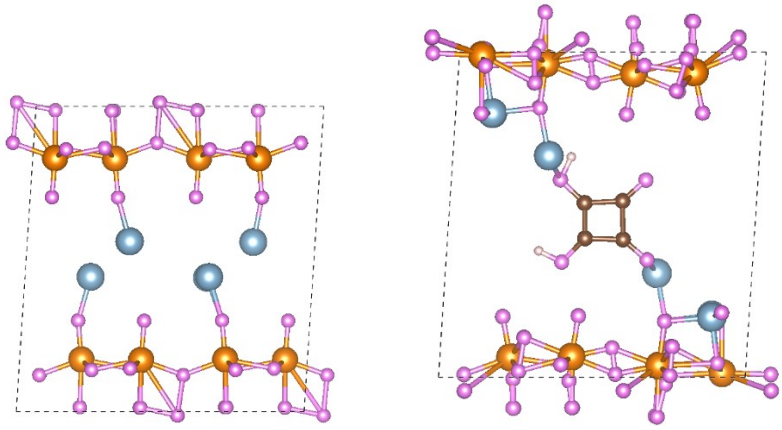

Fig. S9. The structure of HAVO (lift) and HAVO-Sq80 (right).

The initial unit cell of HAVO-Sq80 is based on a typical layered V_3O_8 structure with orthorhombic symmetry, and lattice water in the material was removed during model construction (both HAVO and HAVO-Sq80 contain lattice water, which is not considered here). The structure is composed of VO_6 octahedra and Al^{3+} ions located between the layers. Squaric acid molecules were placed in the interlayer channels of the HAVO host, with the molecules positioned vertically within the interlayer channels before geometric optimization was performed. The main purpose of these DFT calculations is to reveal the general trend and intrinsic mechanism of how squaric acid molecules modulate the electronic structure, interlayer environment, and Zn^{2+} adsorption behavior, rather than to fully fit the precise stoichiometry from experiments.

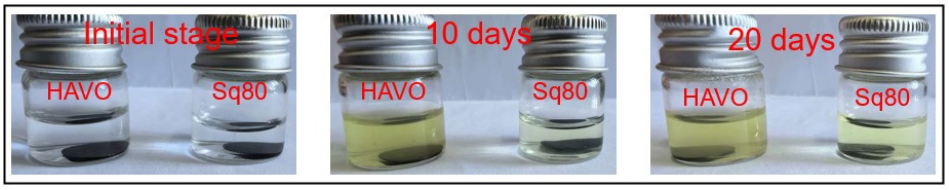

Fig. S10. Optical photo of electrolyte immersed electrodes.

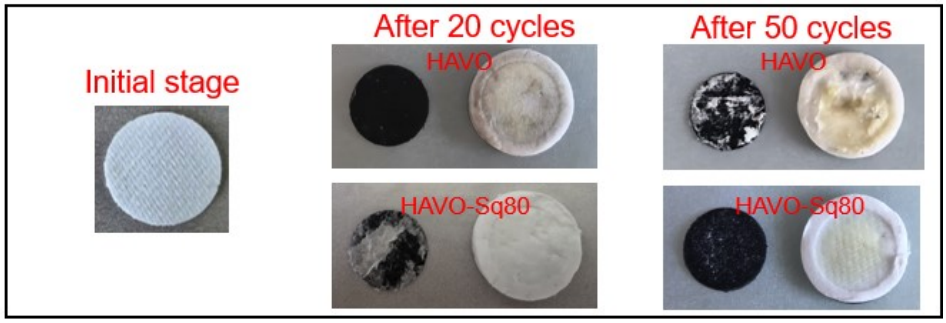

Fig. S11. Optical photo of separator after cycling.

Type	Energy density (Wh kg^{-1})	Loading (mg cm^{-2})	Ref.
Zn-HAVO-Sq80	72	10.6	This work
Zn-V_2O_5	55	4	1
Zn-hybird	25	9	2
Zn-organic	70	3	3
Zn-Te	77	12	4
Zn-Zn_xVOPO_4	45	17	5
Zn-BiO	55	10	6
Zn-FZP	47	11	7
Zn-smSiO_2	65	18	8

[1] J. Heo, K. Shin, H. Kim, et al. Adv. Sci. 2022, 9, e2204908.

[2] S. Gao, B. Li, H. tan, et al. Adv. Mater. 2022, 34, e2201510.

[3] D. Han, C. Cui, K. Zhang, et al. Nat. Sustain. 2022, 5, 205-213.

[4] L. Cao, D. Li, T. Pollard, et al. Nat. Nanotechnol. 2021, 16, 902-910.

[5] Y. Song, l. Shen, X. li, et al. Nat. Chem. Eng. 2024, 1, 588-596.

[6] J. Wan, Z. Qian, J. Xu, et al. Small. 2025, 202411627.

[7] K. Zhao, Y. Wang, et al. Adv. Funct. Mater. 2026, 202501956.

[8] L. Wang, B. Zhang, H. Li, et al. Angew. Inter. Edi. Chem. 2025, 202501010.